A simulation framework for cold-start evaluation of a gasoline engine equipped with an electrically heated three-way catalyst

Citation for the original published paper (version of record):
Velmurugan, D., McKelvey, T., Olsson, J. (2021). A simulation framework for cold-start evaluation of a gasoline engine equipped with an
electrically heated three-way catalyst. IFAC-PapersOnLine, 54(10): 526-533.
http://dx.doi.org/10.1016/j.ifacol.2021.10.216

Available online at www.sciencedirect.com

ScienceDirect

IFAC PapersOnLine 54-10 (2021) 526–533

A simulation framework for cold-start evaluation of a gasoline engine equipped with an electrically heated three-way catalyst ⋆

Dhinesh V. Velmurugan * **Tomas McKelvey** **
Jan-Ola Olsson ***

* *Powertrain Engineering Sweden AB, Gothenburg, Sweden (e-mail: dhinesh.velmurugan@volvocars.com).*
** *Chalmers University of Technology, Gothenburg, Sweden (e-mail: tomas.mckelvey@chalmers.se)*
*** *Powertrain Engineering Sweden AB, Gothenburg, Sweden, (e-mail: jan-ola.olsson@volvocars.com)*

Abstract: Cold start emissions of exhaust gas pollutants in current generation gasoline internal combustion engine (ICE) comprise the most significant quantity of regulated exhaust emissions in both standard test drive cycles and in real-world drive scenarios. Electrification of ICE provides the possibility of using an electrically heated catalyst (EHC), that offers the potential to fulfil future emission legislation such as Eu7. The EHC has the potential to reduce cold start exhaust emission by attaining early and quick catalyst light-off with lower impact on drivability and fuel consumption. A control-oriented simulation model of a gasoline ICE with a two-brick three-way catalyst (TWC) equipped with an EHC between the bricks is described and analysed for use in cold start evaluation of the complete system. The ICE is modelled using a mix of static lookup tables optimized using part load engine test bench measurements, to provide the exhaust emission species flow and gas temperature to the downstream TWC. An axial and radially resolved TWC model, including non-uniform axial lengths of the TWC slices that are relevant for cold start emission control is used. The EHC is modelled as a TWC component with the possibility to generate heat from electrical energy. Significant ICE control measures such as high engine idle, retarded ignition timing and strategic air-fuel ratio that are potentially used for cold start control are emulated. The entire simulation framework is set-up in a manner such that for a given engine speed and torque demand trace, the simulation framework emulates the power-train system. The internal states are modelled to provide fuel consumption and tailpipe exhaust emissions, which would form the significant costs of a cold start controller objective function. A set of proposed heating profiles of the EHC is simulated and available measurements are used for comparison. The resultant framework can estimate the use of engine control measures and the EHC impacts with desired accuracy for carrying out the development and analysis of cold start controller strategies.

Keywords: Cold-Start, Engine exhaust emissions, Hybrid, Engine control, Model

1. INTRODUCTION

Current generation gasoline internal combustion engines (ICE) emit extremely low exhaust pollutant levels of carbon monoxide (CO), total unburned hydrocarbons (THC) and nitrogen oxides (NO_x) under stoichiometric air-fuel ratio (AFR) operation due to the three-way catalyst (TWC). A significant portion of the pollutant emissions that go untreated however, is during the cold start of the ICE. The TWC must attain a catalyst light-off temperature in the order of 250°C to have a high emission conversion efficiency, as established and detailed in B.Heywood (2015).

In order to minimize the cold start exhaust emissions, both engine control measures and catalyst heating devices have been widely reported and applied as summarized in Gao et al. (2019). Most common engine control methods include high engine idle speed, retarded ignition timing and strategically modified AFR control. These engine control methods lead to increased fuel consumption and compromised power availability at engine start.

Additional devices such as the electrically heated catalyst (EHC) could be used without compromise in power availability and reduced impact on total energy consumed. The increased electrification trend in modern ICE equipped passenger cars, which is key to meet CO_2 targets set by regulatory framework, offers an easier implementation due to the availability of increased battery storage capacity

⋆ This work was performed within the Combustion Engine Research Center at Chalmers (CERC) with financial support from the Swedish Energy Agency.

10.1016/j.ifacol.2021.10.216

and a high voltage system on-board, that could deliver more power. See Johnson and Joshi (2017) Knorr et al. (2015).

Due to early catalyst light-off potential possibility by the usage of EHC, lower cold-start exhaust emissions can be achieved, while also reducing the need for limiting the engine power due to catalyst heating. Optimally designed control strategies could potentially lower energy consumption (fuel and electricity), achieve better drivability and result in lower emissions. Electrification of power-trains at different levels combined with EHC devices, could pave the way for development of zero emission impact vehicles as reported in Laurell et al. (2019).

Availability of several subsystems poses a challenge for appropriate control measures to be taken. A control-oriented model of the subsystems involved is necessary for simulation of controllers and their evaluation with a suitable methodology. A wide variety of ICE models are available to use as proposed in Zavala et al. (2007), Andrianov et al. (2010), Verem et al. (2016). In this paper, a simple ICE model developed with data from part load measurements is used. A summary of the model and its performance comparison is presented.

Similarly, plenty of TWC models are available such as Brandt et al. (1997), Pandey et al. (2016), Michel et al. (2017), Koltsakis et al. (1997) which devote a simple TWC model for temperature and emission conversion efficiency prediction. In this paper, a model presented in Lock et al. (2021) is modified to make available non-uniform axially sliced catalyst volumes to enable capturing the catalyst light-off phenomenon and the effect of the EHC on the TWC. EHC models similar to those in Bezaire and Midlam-Mohler (2012) Ramanathan et al. (2011) are used.

The purpose of the proposed simulation framework is to evaluate the performance of different control strategies for the EHC. It could potentially be used as a tool to evaluate different layouts of the catalyst system, however, in this usage it is limited to variations within the validity of the available catalyst models.

2. DESCRIPTION OF THE SETUP

A production Volvo XC90 car with a 4-cylinder 2L turbo and supercharged direct injection gasoline engine that can meet Euro 6d requirements is used. The engine calibration for catalyst heating to provide quick catalyst light-off with high engine idle, retarded ignition timing and AFR adjustment is known and used without modification. The vehicle is instrumented with additional thermocouples and emission measurement sample points both upstream and downstream the catalyst.

The production TWC is replaced by a two-brick TWC with a catalyst coated EHC placed between the two bricks as depicted in Fig. 1. The TWC layout has potential ageing robustness while also providing the possibility of oxygen sensor preheating Laurell et al. (2019). The first TWC brick is a ceramic coated substrate with production like wash-coat precious group metal loading while the second brick is a metallic one that also acts as the supporting matrix for the EHC. The TWC is instrumented with additional thermocouples in several axial center locations and peripheral locations, data from which is used for the TWC models.

The EHC is designed as a heating disc which is mechanically supported by means of supporting pins on the TWC bricks. The heating disc comprises of metallic foils wound into S-shaped forms whose resistance to electrical power applied generates heat in the discs. The $4kW$ EHC in the test vehicle is enabled to be used independent of engine operation, making way for the possibility to pre-heat the catalyst prior to engine start.

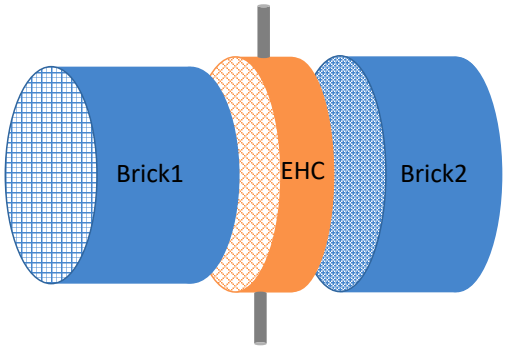

Fig. 1. Brick catalyst configuration used in this paper composed of a ceramic first TWC brick, followed by the EHC and the last metallic TWC brick

3. ENGINE MODEL

A trace of engine speed (N_{eng}) and requested torque (T_{req}) is used as input to the engine and engine control models. The coolant temperature (T_{coolant}) and oil temperature (T_{oil}) are modelled as a function of integrated power demand (from engine start 0 to current sampling instant N) from the engine with a saturation at maintained temperature threshold ($T^{\text{target}}_{\text{coolant}}$, $T^{\text{target}}_{\text{oil}}$) for the fluids tuned using parameter ($x^{factor}_{\text{coolant}}$, x^{factor}_{oil}) as

$$T_{\text{coolant}} = max(T^{\text{target}}_{\text{coolant}}, \sum_{t=0}^{N} x^{factor}_{\text{coolant}} N_{\text{eng}} T_{\text{req}}) \quad (1)$$

$$T_{\text{oil}} = max(T^{\text{target}}_{\text{oil}}, \sum_{t=0}^{N} x^{factor}_{\text{oil}} N_{\text{eng}} T_{\text{req}}) \quad (2)$$

3.1 Engine control measures

The main control measures for mitigation of cold start emissions in the combustion engine include AFR control and ignition timing. Stoichiometric AFR is desired when the catalyst is warm and light-off is achieved. Until such instance, quick catalyst warm-up is enabled with the help of high engine idle speed, retarded ignition timing and operating the engine lean. Engine torque is usually limited by software with a soft restraint and engine efficiency is compromised for the sake of minimising cold start emissions Reif (2014).

A production controller for ignition timing (t_{Ign}), AFR control, fuel-cut off and high engine idle speed is mimicked. Ignition timing map is chosen for a cold start ($t^{\text{Max}}_{\text{Retard}}$) and varied by the scaling factor $\alpha(T_{\text{cat}})$, a function of the catalyst modelled temperature (T_{cat}) until catalyst light-off temperature (T_{warm}) is reached in a significant volume of the catalyst, at which point, a near fuel-optimal maximum brake torque (t_{MBT}) timing can be chosen. For ease of reading, $\alpha(T_{\text{cat}})$ is denoted as α. The ignition timing is chosen as summarised below.

$$t_{\text{Ign}} = \begin{cases} t^{\text{Max}}_{\text{Retard}} & T_{\text{cat}} < T_{\text{cold}} \\ (1-\alpha)t^{\text{Max}}_{\text{Retard}} + \alpha t_{\text{MBT}} & T_{\text{cold}} < T_{\text{cat}} < T_{\text{warm}} \\ t_{\text{MBT}} & T_{\text{warm}} < T_{\text{cat}} \end{cases} \tag{3}$$

AFR is controlled to be lean initially for cold-start and gradually scaled by $\beta(T_{\text{cat}})$, a function of the catalyst modelled temperature (T_{cat}) to oscillate around stoichiometric AFR (Stoich) by a minimal oxygen storage (OSC) model of the catalyst based on Brandt et al. (1997). For ease of reading, $\beta(T_{\text{cat}})$ is denoted as β. The deviations from fuel optimal control are enabled in a scaled manner until catalyst light-off temperature is reached at T_{cat} as

$$\text{AFR} = \begin{cases} \text{lean} & T_{\text{cat}} < T_{\text{cold}} \\ (1-\beta)\text{lean} + \beta\text{Stoich} & T_{\text{cold}} < T_{\text{cat}} < T_{\text{warm}} \\ \text{Stoich} & T_{\text{warm}} < T_{\text{cat}} \end{cases} \tag{4}$$

Fuel cut-off ($B_{\text{Fuel cut}}$) is enabled under low torque requests in addition to fulfilment of certain driving conditions collected in a set of rules (Fuel cut lim) made from vehicle speed (V_{Speed}) and operational gear as shown below

$$B_{\text{Fuel cut}} = \begin{cases} 1, & N_{\text{Eng}} < N^{\text{FC Lim}}_{\text{Eng}} T_{\text{Req}} < T^{\text{FC Lim}}_{\text{Req}} \\ & V_{\text{Speed}}, \text{gear} \in \text{Fuel cut lim} \\ 0, & \text{otherwise} \end{cases} \tag{5}$$

Engine idle speed ($N^{\text{idle}}_{\text{Eng}}$) target is set between high and normal based on reaching the catalyst light-off temperature at T_{cat} as

$$N^{\text{idle}}_{\text{Eng}} = \begin{cases} \text{High} & T_{\text{cat}} < T_{\text{cold}} \\ \text{Normal} & T_{\text{cold}} < T_{\text{cat}} \end{cases} \tag{6}$$

3.2 Engine out emissions

The exhaust gas mass flow ($\dot{m}_{\text{exh}}$) is modelled from a base map of the engine speed (N_{Eng}), requested torque (T_{Req}) and the deviation of the ignition timing (ΔIgn timing) from nominal setting as

$$\dot{m}_{\text{exh}} = f(N_{\text{Eng}}, T_{\text{Req}}) \cdot g(\Delta\text{Ign timing}) \tag{7}$$

with fuel flow estimated as

$$\dot{m}_{\text{fuel}} = \dot{m}_{\text{exh}} * {}^{1}/_{\text{AFR}} \tag{8}$$

A static map of the engine out emissions of carbon monoxide (CO), total unburned hydrocarbons (THC) and oxides of nitrogen (NO_x) is developed for the respective species in consideration. The CO engine out emissions are primarily sensitive to AFR and are modelled as a non-linear function of AFR and fuel cut similar to the approach in Zavala et al. (2007).

A base static map of hydrocarbon emissions as a function of engine speed and load is used. The base map estimate ($\text{base}^{\text{EO}}_{\text{THC}}$) is modified with a quadratic function of the deviation of AFR from stoichiometric value. A base static map ($\text{base}^{\text{EO}}_{\text{NO}_\text{x}}$) of ($\text{NO}_\text{x}$) emissions as a function of engine speed and torque modified similarly based on the deviations in AFR from stoichiometric value is used. The product of the described terms with the exhaust mass flow ($\dot{m}_{\text{exh}}$) provides the modelled exhaust mass flow emission of CO ($\dot{m}^{\text{EO}}_{\text{CO}}$), NO_x ($\dot{m}^{\text{EO}}_{\text{NO}_\text{x}}$) and THC ($\dot{m}^{\text{EO}}_{\text{THC}}$) from the engine summarised as

$$\dot{m}^{\text{EO}}_{\text{CO}} = f(\text{AFR})\dot{m}_{\text{exh}}(1 - B_{\text{Fuel cut}}) \tag{9}$$

$$\begin{aligned} \dot{m}^{\text{EO}}_{\text{NO}_\text{x}} = {} & \text{base}^{\text{EO}}_{\text{NO}_\text{x}}(N_{\text{Eng}}, T_{\text{Req}})\dot{m}_{\text{exh}}(1 - B_{\text{Fuel cut}}) \\ & [(1-AFR)^2 \cdot g(N_{\text{Eng}}, T_{\text{Req}}) \\ & +(1-AFR) \cdot h(N_{\text{Eng}}, T_{\text{Req}}) + 1] \end{aligned} \tag{10}$$

$$\begin{aligned} \dot{m}^{\text{EO}}_{\text{THC}} = {} & \text{base}^{\text{EO}}_{\text{THC}}(N_{\text{Eng}}, T_{\text{Req}})\dot{m}_{\text{exh}}(1 - B_{\text{Fuel cut}}) \\ & [(1-AFR)^2 \cdot g(N_{\text{Eng}}, T_{\text{Req}}) \\ & +(1-AFR) \cdot h(N_{\text{Eng}}, T_{\text{Req}}) + 1] \end{aligned} \tag{11}$$

3.3 Engine out and Catalyst upstream temperature

The catalyst upstream temperature is modelled similar to Verem et al. (2016), Aghaali and Angstrom (2013). A static map of the engine out manifold temperature as a function of engine speed and torque is created from part load engine test measurements, where the manifold temperature ($T_{\text{eng, man}}$) is given by

$$T_{\text{eng, man}} = g(N_{\text{Eng}}, T_{\text{Req}}) \tag{12}$$

The heat loss from the turbocharger is modelled as such as the engine is in nominal operation since the dynamics of the catalyst control are slower than the turbocharger. The catalyst upstream exhaust gas temperature ($T_{\text{eng, ex}}$) and an artificial solid phase temperature (T_{sol}) are estimated with lumped specific heat capacity of the gas ($c_{p,g}$), heat transfer coefficient between solid and exhaust gas ($h_{s,g}$) and area between solid and exhaust gas ($A_{s,g}$) as

$$T_{\text{eng, ex}} = \frac{\dot{m}_{exh} c_{p,g} T_{\text{eng, man}} + h_{sg} A_{sg} T_{sol}}{\dot{m}_{exh} c_{p,g} + h_{s,g} A_{s,g}} \tag{13}$$

with the solid phase (T_{sol}) temperature modelled using the heat transfer coefficient between solid and ambient (h_{sa}), area between solid and ambient (A_{sa}) and a constant ambient temperature (T_{amb}) as

$$\begin{aligned} m_{sol} c_{p,sol} \frac{\text{d}T_{sol}}{\text{d}t} = {} & h_{s,g} A_{s,g} (T_{\text{eng, ex}} - T_{sol}) \\ & + h_{sa} A_{sa} (T_{amb} - T_{sol}) \end{aligned} \tag{14}$$

All the constant parameters used are obtained by minimisation of the square of the error between the measured catalyst upstream temperature and the estimated catalyst upstream temperature.

4. CATALYST MODEL

A control oriented TWC model with axial and radial resolved temperatures based on the axial central and one peripheral temperature deviation is used. Along with an Arrhenius approximated conversion efficiency expression, the heat evolution in the catalyst is based on the individual element temperatures. The model is detailed in Lock et al. (2021). The model has the capability to predict the thermal states and species conversion with as few states as possible, a desired possibility for control-oriented models. Consider N axial segments of a brick with M radial elements, the temperature states (T_n for the n^{th}

axial slice) are listed with all the axial elements and a uniform peripheral temperature deviation (Δ_T). This is used to model the temperature of the elements between each axial center and peripheral position as

$$\bar{T} = [T_1, T_2, ..., T_N, \Delta_T] \tag{15}$$

The corresponding exhaust mass flow in a given radial channel (m) and axial segment (n) is modelled as

$$\dot{m}_{m,1} = \frac{m^2 - (m-1)^2}{M^2}.\dot{m}_{\text{exh}} \tag{16}$$

$$\dot{m}_{m,n+1} = \dot{m}_{m,n} \tag{17}$$

Reactions of CO oxidation, THC oxidation and NO_x reduction commonly accepted as standard in control oriented model generation literature are considered. The reaction rates are modelled using Arrhenius expressions to predict reaction rate k, in any given cell n, m with temperature of the cell ($T_{n,m}$), activation energy (E_a^s) and pre-exponential coefficient (A^s) for each exhaust emission species s as

$$\frac{\mathrm{d}y^s_{n,m}}{\mathrm{d}t} = -k^s_{n,m} y^s_{n,m} \tag{18}$$

$$k^s_{n,m} = A^s e^{\frac{-E^s_a}{RT_{n,m}}} \tag{19}$$

$$y^s_{n,m}(t_r) = y^s_{n,m}(0).e^{-k^s_{n,m} t_r} \tag{20}$$

with residence time t_r calculated as

$$t_r = \frac{V_{\text{slice}}}{\nu} \tag{21}$$

for slice volume V_{slice} and volumetric flow rate ν with mass flow of emitted species for each cell n, m given by

$$\dot{m}^{s,\text{out}}_{n,m} = \dot{m}^{s,\text{in}}_{n,m}.e^{-k^s_{n,m} t_s} \tag{22}$$

where mass flow through each cell is modelled as proportional to frontal area of the respective cell as detailed in Lock et al. (2021). Thus net tailpipe emissions obtained from the last axial segment N as

$$\dot{m}^s_{\text{tp}} = \sum_{m=1}^{M} \dot{m}^{s,\text{out}}_{m,N} \tag{23}$$

The reaction heats from the considered net reactions with constants from NIST are computed for all the three converted emission species s, obtained from the product of the converted species $\dot{m}^{\text{s,conv}}_{n,m}$ with net heat terms $\mathrm{d}H_{\text{s}}$ from the net reactions in each cell n, m, as

$$\begin{aligned} P_{n,m} = {} & \dot{m}^{\text{CO,conv}}_{n,m}.\mathrm{d}H_{\text{CO}} \\ & + \dot{m}^{\text{NO}_\text{x},conv}_{n,m}.\mathrm{d}H_{\text{NO}_\text{x}} \\ & + \dot{m}^{\text{THC,conv}}_{n,m}.\mathrm{d}H_{\text{THC}} \end{aligned} \tag{24}$$

The temperature model composed of thermal conduction ($\bar{T}_{\text{cond}}$), reaction heats ($\bar{T}_{\text{exo}}$), convective heat transfer from exhaust gases ($\bar{T}_{\text{convect}}$) and the heat transfer from the EHC ($\bar{T}_{\text{EHC}}$) using the thermal states, lumped heat coefficients and a diagonal matrix (L) containing the length of the TWC slices is modelled as

$$L\frac{\mathrm{d}\bar{T}}{\mathrm{d}t} = \bar{T}_{\text{cond}} + \bar{T}_{\text{exo}} + \bar{T}_{\text{convect}} + \bar{T}_{\text{EHC}} \tag{25}$$

Axial, radial and ambient thermal conduction terms (τ_{ax}, τ_{ra}, τ_{amb}) are used as tuning parameters. A lumped heat convection parameter τ_{conv} is used for tuning the reaction heat transfer with exothermal power terms at the axial center ($P_{\text{ctr},n}$). A heat convection parameter τ_{convect} is used to tune the heat transferred from the exhaust gas flow axially. The catalysed electric heater is modelled as a catalyst brick with an additional electric heat source. A fit function ($f(\dot{m}_{\text{eng ex}})$) along with a heat transfer coefficient (k_{EHC}), for the heat convection ($\bar{T}_{\text{EHC}}$) when the heater is turned on (with power P_{EHC}) with and without exhaust gas flow is used to enable capturing the thermal effect of the electric heater, since the heater is planned to be used for pre-heating prior to engine start, as well as post engine start. Different patterns of using the EHC can thus be evaluated. The thermal model is composed as

$$\begin{aligned} L\frac{\mathrm{d}\bar{T}}{\mathrm{d}t} = {} & \frac{1}{\tau_{\text{ax}}}\begin{bmatrix} T_2 - T_1 \\ \vdots \\ T_{N-1} - T_N \\ \vdots \\ 0 \end{bmatrix} + \frac{1}{\tau_{\text{ra}}}\begin{bmatrix} \Delta_T \\ \vdots \\ \Delta_T \\ -\Delta_T \end{bmatrix} \\ & + \frac{1}{\tau_{\text{amb}}}\begin{bmatrix} 0 \\ \vdots \\ 0 \\ T_{amb} - \frac{1}{N}\sum_{n=1}^{N}(T_n + \Delta T) \end{bmatrix} \\ & + \frac{1}{\tau_{\text{conv}}}\begin{bmatrix} P_{\text{ctr},1} \\ \vdots \\ P_{\text{ctr},N} \\ \frac{1}{N}\sum_{n=1}^{N}(P_{\text{per},n} - P_{\text{ctr},n}) \end{bmatrix} \\ & + \frac{\dot{m}_{\text{eng ex}}}{\tau_{\text{convect}}}\begin{bmatrix} T_{\text{eng ex}} - T_1 \\ \vdots \\ T_{n-1} - T_n \\ \vdots \\ T_{N-1} - T_N \\ 0 \end{bmatrix} + k_{\text{EHC}} f(\dot{m}_{\text{exh}}) \begin{bmatrix} P_{\text{EHC}} \\ 0 \\ 0 \\ \vdots \\ 0 \end{bmatrix} \end{aligned} \tag{26}$$

The non-uniform slicing of the catalyst brick volumes axially ($l_1, l_2, \cdots, l_N$) enables better capturing the light-off conditions at the frontal face of the catalyst bricks, which is significant to capture the cold start behaviour of the catalyst. The length matrix is composed as

$$\begin{aligned} L = {} & \begin{bmatrix} l_1 & 0 & \cdots & 0 \\ 0 & l_2 & \cdots & 0 \\ & \ddots & & \\ 0 & 0 & \cdots & l_N \end{bmatrix} \\ & s.t. \quad l_1 + \cdots + l_N = 1 \\ & \text{length}_{\text{slice},n} = \text{length}_{\text{cat}} l_n \end{aligned} \tag{27}$$

In this paper, the first brick was modelled as comprising of two non-uniform slices. The EHC and the second TWC brick have been modelled as individual slices. This has been done to increase the accuracy of catalyst light-off activity while keeping the simulation speed high. The axial center and peripheral states are tracked while in-between radial elements are interpolated with a total of 15 radial parts as detailed in Lock et al. (2021). The non-uniform slicing of catalyst bricks affects the slice volumes as

$$V_{\text{slice},n} = \frac{V_{\text{TWC}}}{l_n} \tag{28}$$

4.1 Model tuning

The physical parameters obtained from the catalyst manufacturers such as the volume and cell density are used. The fitting parameters for the thermal coefficients (τ_{ax},τ_{ra},τ_{amb},τ_{conv},τ_{convect}) are obtained using non-linear least squares optimisation of the deviation of the temperatures from the measured temperatures. The brick axial discrete lengths allow a further degree of freedom to tune the model for a more accurate match with the measured temperatures. To tune the electric catalyst heater parameters, measurements from two different patterns of expected EHC usage in the dynamic cycles are used. A $4kW$ EHC heating for $20s$ after the engine has started referred as post heating has been used as a first reference for the EHC tuning. A $4kW$ EHC heating $9s$ prior to the engine start (referred to as pre-heating) and continued upto $20s$ after the engine start is used as the second reference for the EHC tuning. The thermal model parameters (k_{EHC} and $f(\dot{m}_{\text{eng,ex}})$) of the EHC is thus tuned with measurements from both zero-flow conditions (expected pre-heat conditions while ICE is off) and under normal exhaust gas flow through condition (post heat conditions while ICE is in operation) while the EHC is powered up. The chemical model parameters (E_a^s and A^s) for the respective emission species s is tuned with measured temperatures ($T_{\text{n, meas}}(t)$) as input states with a minimisation of the least square error of the estimated emission component ($\dot{m}^s_{\text{tp,est}}(t)$) and the measured species ($\dot{m}^s_{\text{tp, meas}}(t)$). The model tuning was carried out using `patternsearch` and non-linear least squares (`lsqnonlin`) optimisation tool in `Matlab`. The respective species are tuned independently of each other as

$$\min \sum_t \frac{1}{\max(\dot{m}^s_{\text{tp, meas}})}(\dot{m}^s_{\text{tp,est}}(t) - \dot{m}^s_{\text{tp, meas}}(t))^2 \quad (29)$$

The lengths $l_1, l_2, \cdots, l_n$ are chosen initially to be equal. The individual temperatures are tuned with the now tuned chemical parameters to minimise the squared error between the estimated temperatures ($T_{\text{n,est}}(t)$) and the measured temperatures ($T_{\text{n, meas}}(t)$) at each axial temperature location as

$$\min \sum_t \frac{1}{\max(T_{\text{n, meas}})}(T_{\text{n,est}}(t) - T_{\text{n, meas}}(t))^2 \quad (30)$$

In order to attain accurate axial temperature distribution within the same brick, non-uniform segment division is done with the objective of minimising the sum of errors as

$$\begin{aligned}\min \sum_t \frac{1}{\max(\bar{T}_{1:\text{N, meas}})}[&(T_{1,\text{est}}(t) - T_{1,\text{ meas}}(t))^2 \\ &+(T_{2,\text{est}}(t) - T_{2,\text{ meas}}(t))^2 + \cdots \\ &+(T_{\text{N,est}}(t) - T_{\text{N, meas}}(t))^2]\end{aligned} \quad (31)$$

A final refinement of the chemical parameters is necessary due to the redistribution of the volumes.

5. RESULTS

The performance of the described ICE and TWC models described is analysed by comparing to measured data. The predictions of engine cold-start emissions (both instantaneous and accumulated) and catalyst temperatures are the significant predicted outputs that are compared for evaluating the simulation framework.

5.1 Comparison of Engine Out Emissions

The predicted and measured engine exhaust emissions of CO, THC and NO_x are compared. The prediction of the emission species depends to a good degree upon the successful reproduction of engine control measures. To illustrate the captured production controls and the difference between the emulated and actual control, the model is simulated using the recorded control signals also, to portray a good comparison. The accuracy of the predicted CO emissions depend on the accuracy of the controlled AFR between the measurements and the simulation, the effect of which can be clearly seen in the comparison plots from Fig. 2 to Fig. 5. The THC and NO_x are predicted with a higher accuracy due to the dependence on the base map more significantly. The overall trend and phenomenon are captured by the models with reasonable accuracy for the purpose of this paper.

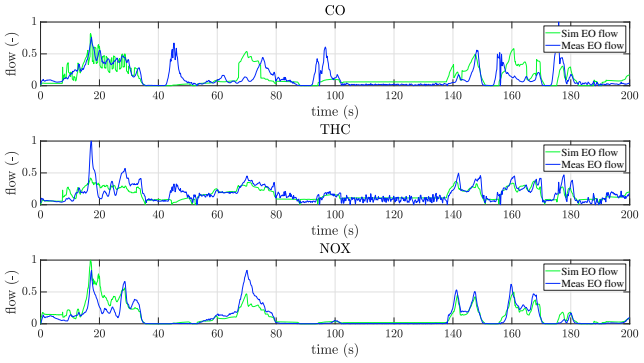

Fig. 2. Instantaneous engine out exhaust emissions flow with simulated engine controls compared to measurements normalised with the maximum of the respective flows.

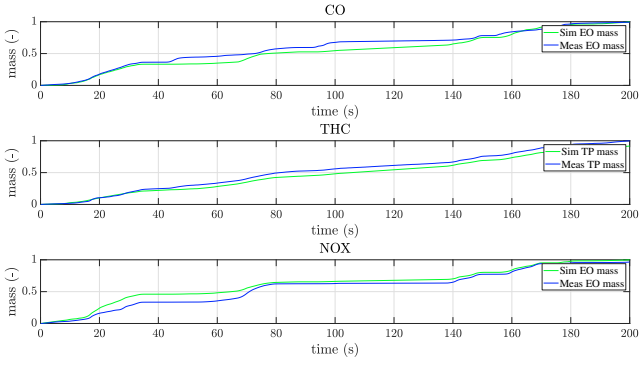

Fig. 3. Accumulated engine out exhaust emissions with simulated engine controls compared to measurements normalised with the maximum of the respective emission mass.

5.2 Fuel Consumption

Fuel consumption simulated from the emulated controller and the recorded control signal is shown in Fig. 6 and 7. The deviations during the catalyst start need some refinement to capture the loss of engine efficiency much more accurately.

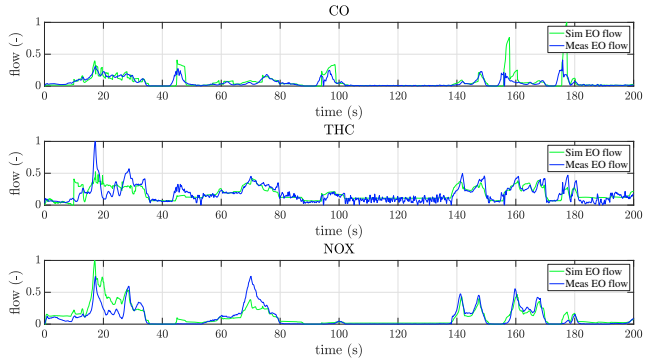

Fig. 4. Instantaneous engine out exhaust emissions with recorded engine controls compared to measurements normalised with the maximum of the respective flows.

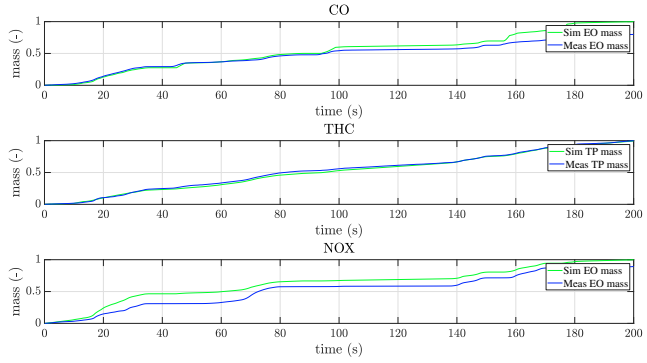

Fig. 5. Accumulated engine out exhaust emissions with recorded engine controls compared to measurements normalised with the maximum of the respective emission mass.

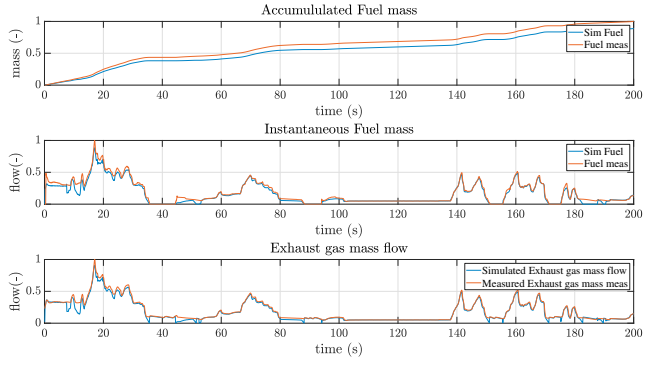

Fig. 6. Fuel consumption and exhaust mass flow with simulated engine controls compared to measurements, normalised with respective flow and mass

5.3 Catalyst gas upstream temperature

Comparison of predicted exhaust gas catalyst upstream temperature and the corresponding thermocouple measurement is shown in Fig.8. The accuracy of the prediction is deemed to be good for the purpose of the paper.

5.4 Comparison of Temperature evolution from Engine to Tailpipe

The temperature of the axial elements of the considered model is compared to the corresponding closest thermocouple measurement. The model is fed with upstream

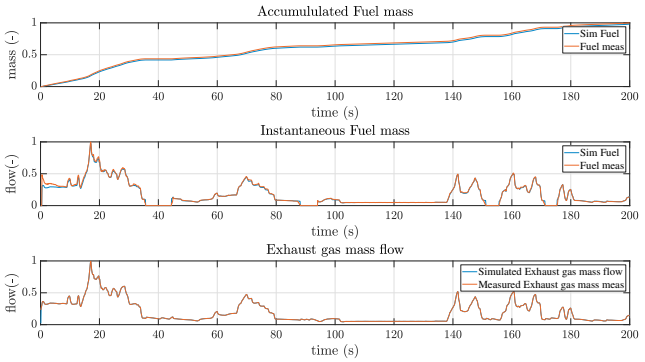

Fig. 7. Fuel consumption and exhaust mass flow with recorded engine controls compared to measurements, normalised with respective flow and mass

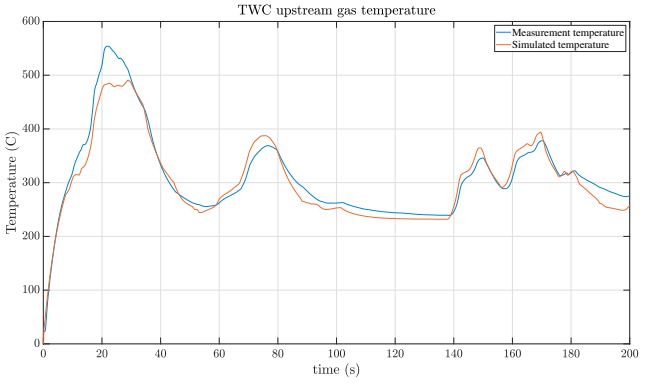

Fig. 8. Simulated catalyst gas upstream temperature compared to measured temperature.

measurements of the emission species, exhaust mass flow and the exhaust gas upstream TWC temperature. The temperature evolution is compared for three cases: 1. The EHC is turned off, 2. EHC $4kW$ heating is run for $20s$ following engine start and 3. EHC $4kW$ heating is run for $9s$ prior to engine start and $20s$ following engine start. The cases under consideration are arranged back to back and visualised with the engine speed and the EHC power trace in Fig.9. A thermocouple was not present directly on the

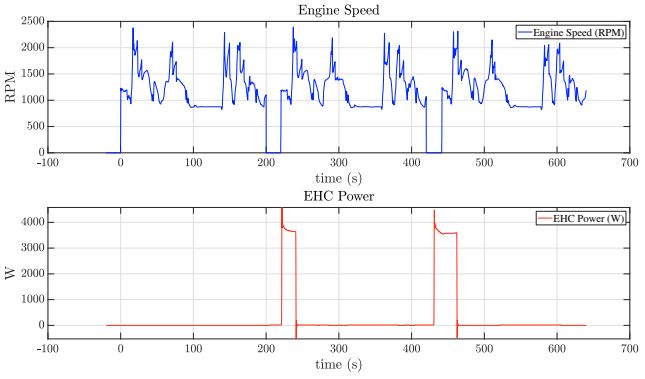

Fig. 9. Engine Speed and EHC power trace for the three cases arranged back to back

EHC in the test object and hence closest thermocouples have been compared. A re-loop tuning of the TWC parameters would increase accuracy due to exothermic reactions from the exhaust species. The resultant accuracy as shown

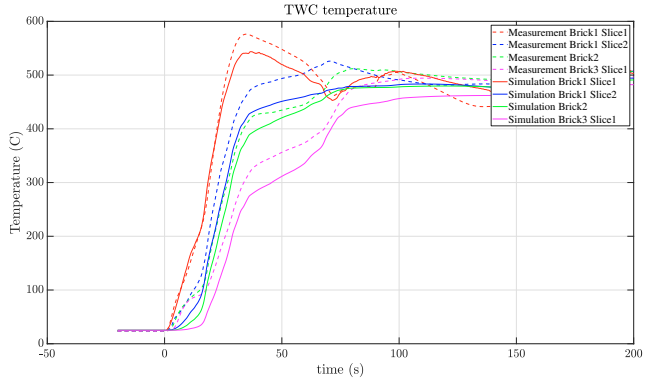

Fig. 10. Axial temperature evolution in the respective TWC slices with EHC turned off

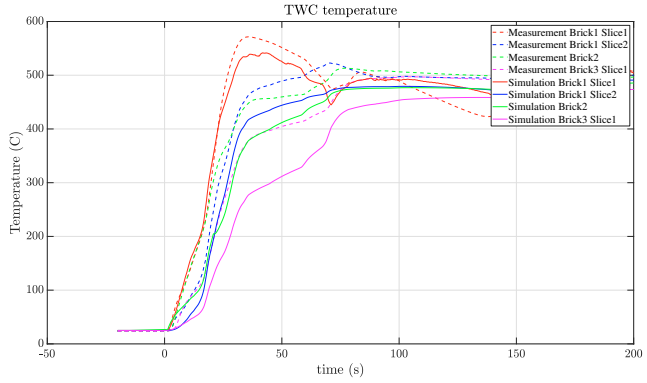

Fig. 11. Axial temperature evolution in the respective TWC slices with EHC post heat

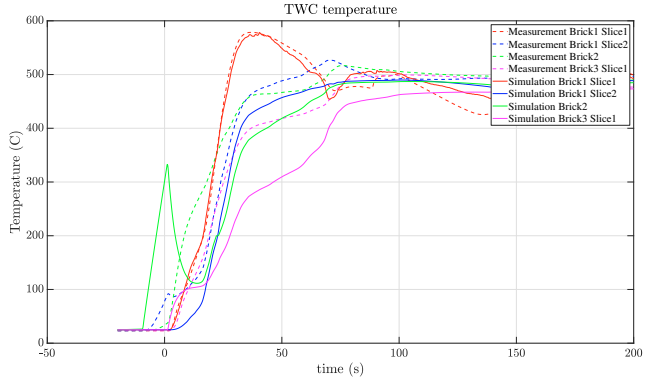

Fig. 12. Axial temperature evolution in the respective TWC slices with EHC pre heat

in Fig.10, Fig.11 and Fig.12 is deemed to capture the desired thermal accuracy necessary for the intent of the paper.

5.5 Comparison of Tailpipe emissions

The tailpipe emissions of CO, THC and NO_x are compared for the three cases of the EHC usage with accumulated emissions shown in Figs. 13 and 14 and instantaneous emissions shown in Figs. 15, 16 and 17. It can be noticed that the effect of the EHC on NO_x reduction is small in comparison to the effect on CO and THC. The trend is reflected appropriately in both the instantaneous tailpipe comparison and overall accumulated emissions reduction

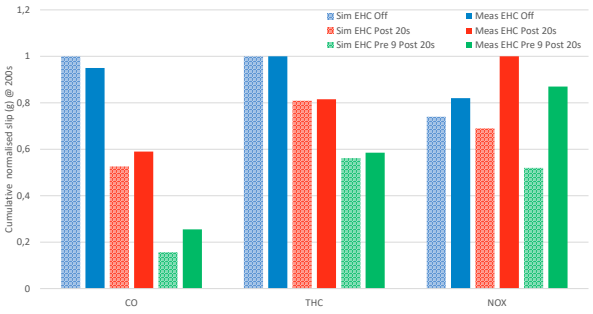

Fig. 13. Comparison of measured and simulated total accumulated tailpipe emissions for the different EHC usage patterns, normalised with respective emissions mass

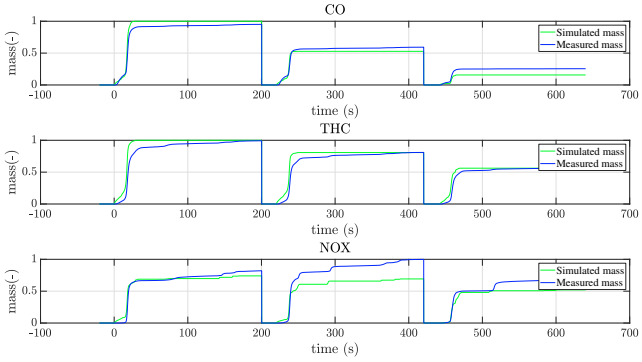

Fig. 14. Comparison of measured and simulated accumulated evolution of tailpipe emissions, normalised with the respective emissions mass

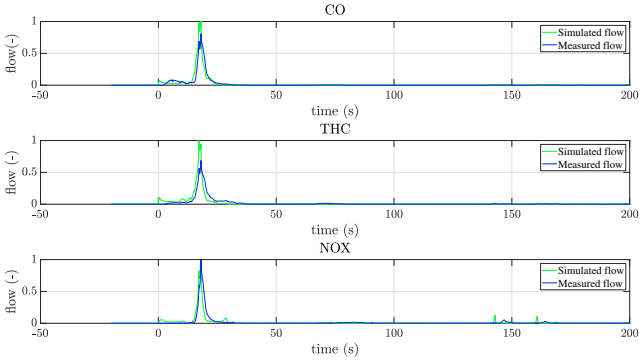

Fig. 15. Comparison of measured and simulated instantaneous tailpipe emissions with EHC off, normalised with the respective emissions mass flow

trend with usage of the EHC. While the NO_x measurement shown here has been used, investigation is necessary for the reason behind the moderate increase in NO_x slip with usage of the EHC. A hypothesis is that this could be the effect of a higher and earlier accumulated oxygen storage, due to the heating of the EHC, further increased due to the lean engine AFR strategy for catalyst warming. The model is able to predict a comparable reduction in exhaust emissions due to activity of the heater. The comparison of exhaust emission slip is shown for the measured and the simulated cumulative tailpipe exhaust emissions mass at the end of 200s summarised in Fig.13.

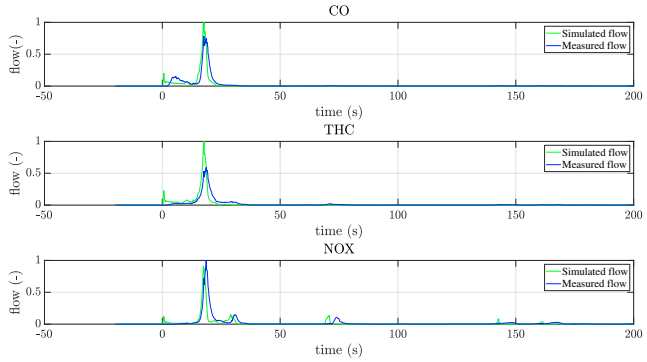

Fig. 16. Comparison of measured and simulated instantaneous tailpipe emissions with EHC post heat, normalised with the respective emissions mass flow

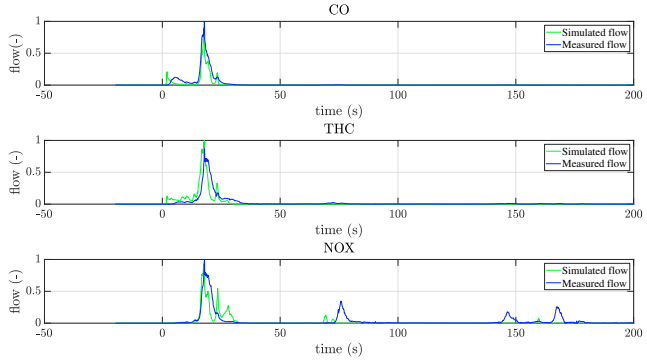

Fig. 17. Comparison of measured and simulated instantaneous tailpipe emissions for EHC pre heat, normalised with the respective emissions mass flow

6. CONCLUSION

The simulation speed of the combined models is 100 times faster than real-time without any optimisation effort taken for speed increase. The assumed conversion efficiency distribution between the bricks and the slices can be refined with the help of additional measurements between the different catalyst bricks. The temperature predictions could be improved with the help of additional measurement on the catalyst heater. However, even with the availability of measurements upstream and downstream the catalyst under different heated profiles provides a good estimate at the distribution as noticed in the net resulting emissions prediction and temperature prediction accuracy. The engine out emissions, temperature and fuel consumption have been predicted with an accuracy deemed to be acceptable for the purpose of evaluating cold start control strategies with the capturing of the effect of the significant cold start engine control measures commonly used.

REFERENCES

Aghaali, H. and Angstrom, H.E. (2013). Temperature estimation of turbocharger working fluids and walls under different engine loads and heat transfer conditions. *SAE Technical Papers*. doi:10.4271/2013-24-0123.

Andrianov, D.I., Keynejad, F., Dingli, R., Voice, G., Brear, M.J., and Manzie, C. (2010). A cold-start emissions model of an engine and aftertreatment system for optimisation studies. *SAE Technical Papers*. doi:10.4271/2010-01-1274.

Bezaire, B. and Midlam-Mohler, S. (2012). A Physically-Based, Lumped-Parameter Model of an Electrically-Heated Three-Way Catalytic Converter. *SAE Technical Paper Series*, 1. doi:10.4271/2012-01-1240.

B.Heywood, J. (2015). *Internal Combustion Engine Fundamentals Second Edition*. New York, McGrawHill.

Brandt, E.P., Wang, Y., and Grizzle, J.W. (1997). Simplified three-way catalyst model for use in on-board SI engine control and diagnostics. *American Society of Mechanical Engineers, Dynamic Systems and Control Division (Publication) DSC*, 61, 653–659.

Gao, J., Tian, G., Sorniotti, A., Karci, A.E., and Di Palo, R. (2019). Review of thermal management of catalytic converters to decrease engine emissions during cold start and warm up. *Applied Thermal Engineering*, 147, 177–187. doi:10.1016/j.applthermaleng.2018.10.037.

Johnson, T. and Joshi, A. (2017). Review of Vehicle Engine Efficiency and Emissions. *SAE Technical Papers*, 2017-March. doi:10.4271/2017-01-0907.

Knorr, T., Ellmer, D., Maiwald, O., Schatz, A., and Brück, R. (2015). The Electric Heatable Catalyst – An Efficient Measure for Emission Optimization in Mild Hybrid Vehicle Operation Strategies. *24th Aachen Colloquium Automobile and Engine Technology*, 1–22.

Koltsakis, G.C., Konstantinidis, P.A., and Stamatelos, A.M. (1997). Development and application range of mathematical models for 3-way catalytic converters. *Applied Catalysis B: Environmental*, 12(2-3), 161–191. doi:10.1016/S0926-3373(96)00073-2.

Laurell, M., Pace, L., Ekström, F., and Konieczny, K. (2019). Strive for Zero Emissions Impact from Hybrids. *SAE Technical Papers*, (September). doi:10.4271/2019-24-0146.

Lock, J., Clasen, K., Sjoblom, J., and Mckelvey, T. (2021). A Spatially Resolved Control-Oriented Thermal Model of the Three-Way-Catalyst. In *SAE Technical Papers*. doi:doi:10.4271/2021-01-0597.

Michel, P., Charlet, A., Colin, G., Chamaillard, Y., Bloch, G., and Nouillant, C. (2017). Optimizing fuel consumption and pollutant emissions of gasoline-HEV with catalytic converter. *Control Engineering Practice*, 61, 198–205. doi:10.1016/j.conengprac.2015.12.010.

Pandey, V., Jeanneret, B., Gillet, S., Keromnes, A., and Moyne, L.L. (2016). A simplified thermal model for the three way catalytic converter. *21st International Transport and Air Pollution Conference*.

Ramanathan, K., Oh, S.H., and Bissett, E.J. (2011). Electrically Heated Catalysts for Hybrid Applications: Mathematical Modeling and Analysis. *Industrial & Engineering Chemistry Research*, 50(14), 8444–8467. doi:10.1021/ie200044w.

Reif, K. (2014). *Gasoline Engine Management Bosch Professional Automotive Information*.

Verem, A., Kerai, H., and Larsson, M. (2016). Physically Based Models for Predicting Exhaust Temperatures in SI Engines.

Zavala, J.C., Sanketi, P.R., Wilcutts, M., Kaga, T., and Hedrick, J.K. (2007). Simplified models of engine hc emissions, exhaust temperature and catalyst temperature for automotive coldstart. In *IFAC Proceedings Volumes (IFAC-PapersOnline)*, volume 5, 199–206. doi:10.3182/20070820-3-us-2918.00028.